

# Systematic and controllable negative, zero and positive thermal expansion in cubic $\text{Zr}_{1-x}\text{Sn}_x\text{Mo}_2\text{O}_8$

Sarah E. Tallentire<sup>1</sup>, Felicity Child<sup>1</sup>, Ian Fall<sup>1</sup>, Liana Vella-Zarb<sup>1</sup>, Ivana Radosavljević Evans<sup>1</sup>, Matthew G. Tucker<sup>2</sup>, David A. Keen<sup>2</sup>, Claire Wilson<sup>3</sup>, John S.O. Evans<sup>1\*</sup>

<sup>1</sup>Department of Chemistry, Durham University, Science Laboratories, South Road, Durham, UK, DH1 3LE; <sup>2</sup>ISIS Neutron and Muon Source, Science and Technology Facilities Council, Rutherford Appleton Laboratory, Harwell Oxford, Didcot, UK, OX11 0QX; <sup>3</sup>Diamond Light Source, Didcot OX11 0DE, Oxon, England.

---

**ABSTRACT:** We describe the synthesis and characterization of a family of materials,  $\text{Zr}_{1-x}\text{Sn}_x\text{Mo}_2\text{O}_8$  ( $0 < x < 1$ ) whose isotropic thermal expansion coefficient can be systematically varied from negative to zero to positive values. These materials allow tunable expansion in a single phase as opposed to using a composite system. Linear thermal expansion coefficients,  $\alpha_i$ , ranging from  $-7.9(2) \times 10^{-6} \text{ K}^{-1}$  to  $+5.9(2) \times 10^{-6} \text{ K}^{-1}$  (12 to 500 K) can be achieved across the series; contraction and expansion limits are of the same order of magnitude as the expansion of typical ceramics. We also report the various structures and thermal expansion of “cubic”  $\text{SnMo}_2\text{O}_8$ , and use time- and temperature-dependent diffraction studies to describe a series of phase transitions between different ordered and disordered states of this material.

---

## INTRODUCTION

In recent years there has been significant interest in phases which show a bulk contraction in volume on heating, so called negative thermal expansion (NTE) materials.<sup>1-5</sup> One of the main reasons for this interest is the possibility of using NTE phases in conjunction with normal positive thermal expansion (PTE) phases to produce composites with controllable negative, positive or even zero thermal expansion (ZTE). Such composites have a range of potential applications where high precision thermal control is needed. The expansion properties and lifetimes of ZTE composites will, however, depend critically on their microstructure, and the inevitable stresses caused at interfaces between expanding and contracting components can lead to failure. The ability to systematically control the thermal expansion of a single phase over a range of values from NTE to PTE, including ZTE, over a wide temperature range would therefore offer a significant step forward. In this paper we report how such control can be achieved in the isotropic  $\text{Zr}_{1-x}\text{Sn}_x\text{Mo}_2\text{O}_8$  system. We also report the fascinating structural chemistry of  $\text{SnMo}_2\text{O}_8$  which underpins this behavior.

Most materials show positive thermal expansion with linear expansion coefficients typically around  $+5-20 \times 10^{-6} \text{ K}^{-1}$  for metals and ceramics. PTE can ultimately be traced back to the asymmetric nature of a typical interatomic potential, which leads to bond expansion as higher energy vibrational levels are populated. Mechanisms which can give rise to NTE or ZTE over either narrow or extended temperature ranges include valence state or other electronic transitions (e.g.  $\text{Sm}_3\text{C}_{60}$ <sup>6</sup>,  $\text{BiNiO}_3$ <sup>7</sup>,  $\text{YbGaGe}$ <sup>8,9</sup>), magnetic transitions (e.g. the INVAR effect<sup>10</sup>,  $\text{Mn}_3\text{Cu}_{1-x}\text{Ge}_x\text{N}^{11}$ ,  $\text{CuO}$  and  $\text{MnF}_2$ <sup>12</sup>), and crystal field/electronic effects at low temperature<sup>2</sup>. Near-zero thermal expansion has been achieved in anti-perovskites such as  $\text{Mn}_3\text{Cu}_{1-x}\text{Sn}_x\text{N}_{1-\delta}$  where a volume-contracting magnetic phase transition counteracts the under-

lying positive thermal expansion close to the Néel temperature of the material.<sup>4,13</sup> The effect is, however, restricted to a relatively narrow temperature range.

The most common origin of NTE over a wide temperature range is phonon-related and a number of materials (framework oxides and cyanides, zeolites, metal organic frameworks) have been shown to display phonon-driven contraction.<sup>2,14</sup> Here the population of negative-Grüneisen-parameter modes on heating, such as those caused by transverse vibrations of M–O–M linkages, brings the metals of the framework closer together. The ultra-low thermal expansion materials  $\text{TaO}_2\text{F}$  ( $\alpha_i$  varying from  $-1$  to  $+1 \times 10^{-6} \text{ K}^{-1}$  from 25–600 °C) owes its behavior to this mechanism.<sup>15-17</sup>

The best known NTE oxides are the cubic  $\text{AM}_2\text{O}_8$  family ( $A = \text{Zr}, \text{Hf}; M = \text{Mo}, \text{W}$ ; Figure 1) which show isotropic NTE over a wide temperature range.<sup>18-21</sup>  $\text{ZrW}_2\text{O}_8$  itself shows isotropic NTE from 2–1070 K with a linear expansion coefficient  $\alpha_i$  of  $-9.0 \times 10^{-6} \text{ K}^{-1}$  (0–350 K). All materials with the basic topology shown in Figure 1 have been reported to exhibit NTE and this has been related to the flexible structure of the network of corner sharing  $\text{AO}_6$  octahedra and  $\text{MO}_4$  tetrahedra. This topology supports a family of low-energy negative-Grüneisen-parameter modes,<sup>22</sup> which can be described within the (quasi) Rigid Unit Mode (qRUM or RUM) language of Dove and co-workers.<sup>23-25</sup>

There have been many attempts to systematically tune the thermal expansion properties of  $\text{AM}_2\text{O}_8$  materials via chemical substitution though these have had limited success. The phase diagrams of the  $\text{ZrW}_2\text{O}_8$  and  $\text{ZrMo}_2\text{O}_8$  systems are such that the cubic phases are only thermodynamically stable in a narrow temperature window (1378–1530 K for  $\text{ZrW}_2\text{O}_8$ ; ~1400 K for  $\text{ZrMo}_2\text{O}_8$ ).<sup>26,27</sup> For  $\text{ZrW}_2\text{O}_8$  the binary oxides are stable at lower temperatures, whereas for  $\text{ZrMo}_2\text{O}_8$  two PTE polymorphs (the monoclinic  $\alpha$ - and trigonal  $\beta$ -) are

more stable than the cubic form. The synthesis of Mo-containing systems is further complicated by the volatility of  $\text{MoO}_3$  at high temperatures and careful low temperature precursor-based routes are required for their preparation. With the exception of Hf, substitutions reported to date on the A site show a limited range of solubility:  $\text{Zr}_{1-x}\text{Sn}_x\text{W}_2\text{O}_8$  ( $x \leq 0.2$ ),  $\text{Zr}_{1-x}\text{Ti}_x$  ( $\leq 0.05$ ) and  $\text{Zr}_{1-x}\text{Ln}_x$  ( $x \leq 0.05$ ;  $\text{Ln}^{3+} = \text{Sc}, \text{Y}, \text{In}, \text{Eu}, \text{Er}, \text{Yb}, \text{Lu}$ ).<sup>28-36</sup> The thermal contraction properties on substitution are largely unchanged, though the temperature of the  $\alpha$ - $\beta$  phase transition (see below) can be altered influencing lower-temperature expansion.

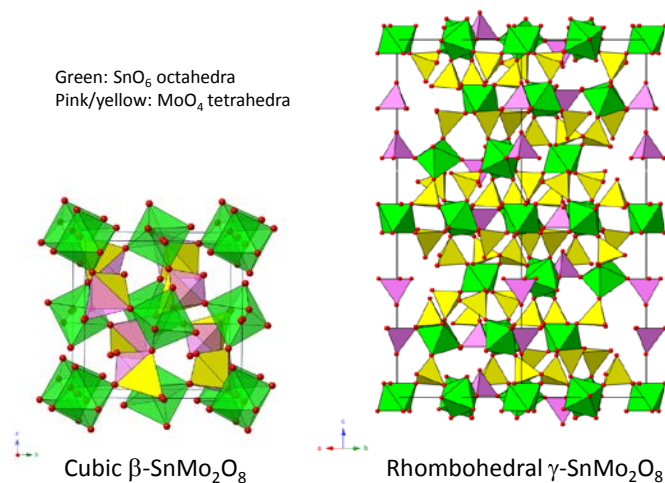


**Figure 1.** Structures of cubic  $\beta\text{-SnMo}_2\text{O}_8$  and rhombohedral  $\gamma\text{-SnMo}_2\text{O}_8$ .  $\text{SnO}_6$  octahedra shown in green,  $\text{MoO}_4$  tetrahedra in yellow/pink. At high temperature  $\beta\text{-SnMo}_2\text{O}_8$  tetrahedra are dynamically disordered over the yellow/pink sites; the yellow sites are those that would be occupied in ordered  $\text{P2}_13$   $\alpha\text{-ZrW}_2\text{O}_8$ . In ordered rhombohedral  $\gamma\text{-SnMo}_2\text{O}_8$  occupied tetrahedral orientations are shaded as yellow (same) or pink (reversed) to show their orientation relative to those in  $\alpha\text{-ZrW}_2\text{O}_8$ .

Due to synthetic challenges, no significant control of thermal expansion via A site substitution in the  $\text{ZrMo}_2\text{O}_8$  system has been reported. However size considerations and the crystal chemistry of related systems suggest that a cubic Sn-substituted system should be at least kinetically stable. The literature relating to the oxygen rich part of the Sn-O-Mo system is a little confused. A stable (500–903 °C)  $\text{SnMo}_2\text{O}_8$  phase was claimed by early workers<sup>37</sup> though others have failed to reproduce this, suggesting the sample was a binary oxide mixture.<sup>38,39</sup> There have, however, been two reports of the preparation of  $\text{SnMo}_2\text{O}_8$  with a structure related to cubic  $\text{ZrMo}_2\text{O}_8$  via a low temperature route which involves flowing  $\text{SnCl}_4$  vapor in an  $\text{O}_2$  carrier gas over solid  $\text{MoO}_3$ .<sup>39,40</sup> Little information has appeared on this material and neither its physical properties nor its potential influence on NTE systems have been investigated. In this paper we report the development of a reliable and reproducible way to produce phase-pure  $\text{SnMo}_2\text{O}_8$  for the first time, allowing us to determine its complex structural landscape.  $\text{SnMo}_2\text{O}_8$  is remarkable in the cubic  $\text{AM}_2\text{O}_8$  family in that it has positive thermal expansion. We also report how this development leads to the ability to form a solid solution,  $\text{Zr}_{1-x}\text{Sn}_x\text{Mo}_2\text{O}_8$ , which has a completely tunable thermal expansion from positive to negative, including near zero-expansion compositions. We thus reveal an unprecedented level of chemical control of thermal

expansion (NTE, ZTE, PTE) in a single phase over a very wide temperature range.

## EXPERIMENTAL SECTION

**Synthesis.**  $\alpha\text{-SnMo}_2\text{O}_8$  was prepared by two routes. Using the method of Buiten,<sup>40</sup> we could prepare the phase over a temperature range of 773 to 873 K with up to 90% pure samples (impurities ~5%  $\text{SnO}_2$ , ~5%  $\text{MoO}_3$ ) formed after 7 h of heating at 773 K. Cubic materials  $\text{Zr}_{1-x}\text{Sn}_x\text{Mo}_2\text{O}_8$  over the range  $0.2 \leq x \leq 1$  were also prepared by a coprecipitation route followed by controlled annealing of the amorphous product. In a typical synthesis ( $x = 0.5$ ) 1.0522 g of  $\text{SnCl}_4 \cdot 5\text{H}_2\text{O}$  (3.0 mmol, 98%, Aldrich) and 0.9660 g of  $\text{ZrOCl}_2 \cdot 8\text{H}_2\text{O}$  (3.0 mmol, 98%, Aldrich) were dissolved in 12  $\text{cm}^3$  of distilled water to form a colorless solution. 2.1374 g of  $(\text{NH}_4)_6\text{Mo}_7\text{O}_{24} \cdot 4.89\text{H}_2\text{O}$  (1.71 mmol, 99.999%, Alfa Aesar) was dissolved in 12  $\text{cm}^3$  of distilled water to form a colorless solution. The two solutions were added alternately drop-wise to 6  $\text{cm}^3$  of distilled water with continuous stirring. A purple/grey precipitate formed immediately and the suspension was stirred overnight. The precipitate was dried in an oven at 323 K to obtain a lilac amorphous solid. Pale yellow crystalline cubic  $\text{Zr}_{1-x}\text{Sn}_x\text{Mo}_2\text{O}_8$  was obtained by heating at 2 K/min to 853 K, and holding for 0.5 h.

**Powder diffraction.** Variable temperature diffraction data were collected in Bragg-Brentano geometry on a Bruker d8 diffractometer equipped with a LynxEye linear position sensitive detector using  $\text{Cu K}\alpha_{1/2}$  radiation. High temperature data were collected using an Anton-Paar HTK1200 environmental heating chamber. Temperature calibration was checked using an  $\text{Al}_2\text{O}_3$  internal standard following a published protocol.<sup>41</sup> Low temperature data were collected using an Oxford Cryosystems pHenIX cryostat. Quench-hold diffraction data of Figure 4 were collected on a sample mounted in a 0.3 mm capillary and recorded in transmission mode on a Bruker d8 diffractometer fitted with a parallel-beam Göbel mirror. The sample was cooled using an Oxford Cryosystems cobra cryostream, and temperature calibration confirmed using an external standard.

For the in-situ data collected during sample synthesis in Figure 3b (and similar experiments for  $0.2 \leq x \leq 1.0$ ) quantitative Rietveld refinement was performed using the 7 different crystalline phases that were observed during the synthesis of the whole  $\text{Zr}_{1-x}\text{Sn}_x\text{Mo}_2\text{O}_8$  series. The amount of amorphous material was estimated by mixing 25% by mass of crystalline  $\text{Al}_2\text{O}_3$  with each sample. Due to the absorption difference between the standard and other phases a Brindley correction was applied during refinement. An appropriate value for the correction (corresponding to 4  $\mu\text{m}$  particles) was determined by analyzing a known mixture of  $\text{Al}_2\text{O}_3$ ,  $\text{ZrO}_2$  and  $\text{MoO}_3$ . Due to reactivity with components we could not use standards with a closer absorption coefficient.

All Rietveld refinements were performed with the Topas Academic software suite. Selected refinement results are given in the figure captions and main text. Full crystallographic details are given in Supporting Information.

## RESULTS AND DISCUSSION

**Thermal Expansion of cubic  $\text{SnMo}_2\text{O}_8$ .** Powder diffraction of a sample of cubic  $\text{SnMo}_2\text{O}_8$  prepared by the method of Buiten<sup>40</sup> confirmed the structure was closely related to cubic  $\text{ZrMo}_2\text{O}_8$  (see Supporting Information Figure S1 and

Figure 5b). We call the room temperature form of this material  $\alpha$ - $\text{SnMo}_2\text{O}_8$ . The thermal expansion of  $\alpha$ - $\text{SnMo}_2\text{O}_8$  is shown in Figure 2a in comparison to other  $\text{AM}_2\text{O}_8$  materials.  $\alpha$ - $\text{SnMo}_2\text{O}_8$  is unique among cubic  $\text{AM}_2\text{O}_8$  systems in that it shows a positive expansion coefficient;  $\alpha_i$  is  $+1.0 \times 10^{-5} \text{ K}^{-1}$  from  $-100$  to  $+100^\circ\text{C}$  compared to  $-7.8 \times 10^{-6} \text{ K}^{-1}$  for  $\alpha$ - $\text{ZrW}_2\text{O}_8$  over the same range. From around 330 K  $\alpha$ - $\text{SnMo}_2\text{O}_8$  undergoes a volume-increasing ( $\Delta V \sim +0.6\%$ ) phase transition. Changes in the powder diffraction pattern through this phase transition are minimal (Supporting Information Figure S2) suggesting minimal structural changes. This phase transition is explored in more detail below.

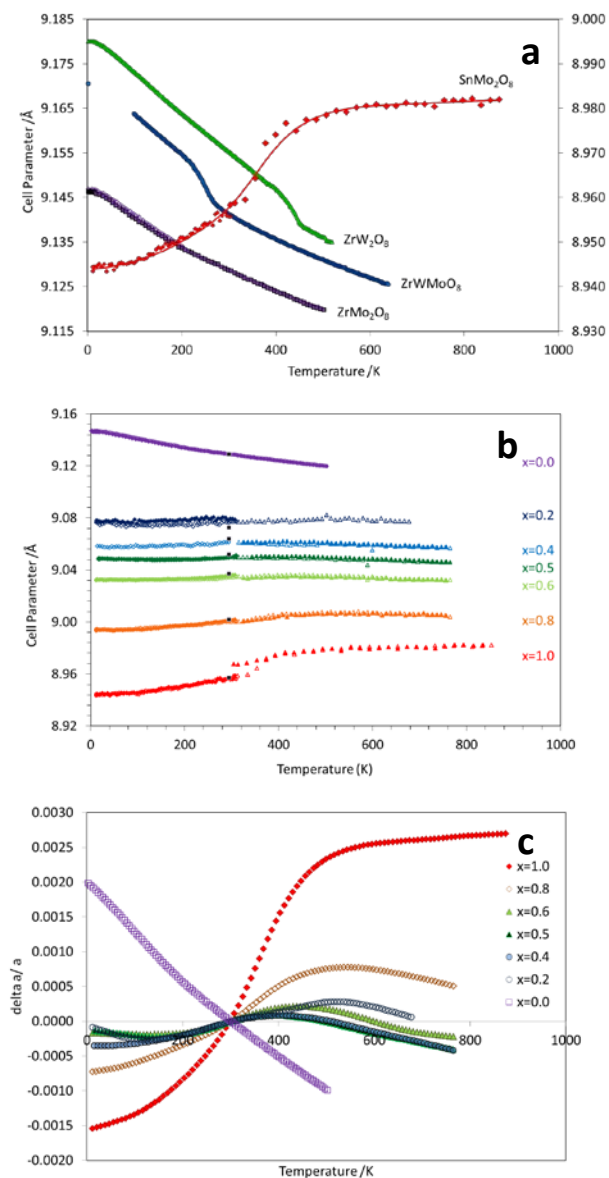


**Figure 2.** Thermal expansion of  $\text{Zr}_{1-x}\text{Sn}_x\text{Mo}_2\text{O}_8$ . **a**, unit cell parameters for cubic  $\text{ZrW}_2\text{O}_8$ ,  $\text{ZrWMoO}_8$  and  $\text{ZrMo}_2\text{O}_8$  (left hand axis) and  $\alpha/\beta$ - $\text{SnMo}_2\text{O}_8$  (right hand axis). **b**, cell parameters extracted from powder diffraction data collected on warming (open symbols) and cooling (closed symbols)  $\text{Zr}_{1-x}\text{Sn}_x\text{Mo}_2\text{O}_8$  materials in a cryostat (circles) or furnace (triangles). Closed black squares are 300 K cell parameters determined using a Si internal standard. Small calibration offsets of furnace data have been applied to match 300 K cells (0.0017,

0.005, 0.0036, 0.0027, 0.0019 & 0.0044 Å for  $x = 0.2, 0.4, 0.5, 0.6, 0.8$  and 1.0). **c**, thermal expansion data in the form  $(a_T - a_{300})/a_{300} \text{ K}$  for  $\text{Zr}_{1-x}\text{Sn}_x\text{Mo}_2\text{O}_8$  materials derived from spline fitting of data in **b**.

### Synthesis and Thermal Expansion of $\text{Zr}_{1-x}\text{Sn}_x\text{Mo}_2\text{O}_8$ .

Due to difficulties with the reproducibility of the flow synthesis of  $\alpha$ - $\text{SnMo}_2\text{O}_8$  (control of the flow rate, reagent surface area,  $\text{MoO}_3$  &  $\text{Mo}_2\text{O}_7\text{Cl}_2$  volatility, ubiquitous presence of impurities, etc.) we have developed an alternate low temperature synthesis. Initially a precursor is formed via the coprecipitation of  $\text{SnCl}_4 \cdot 5\text{H}_2\text{O}$  and  $(\text{NH}_4)_6\text{Mo}_7\text{O}_{24} \cdot 4.5\text{H}_2\text{O}$  solutions to form an amorphous  $\text{SnMo}_2\text{O}_y(\text{OH})_{16-2-y} \cdot n\text{H}_2\text{O}$  material. Heating this material to 863 K for 0.5 h led to a high purity sample of  $\alpha$ - $\text{SnMo}_2\text{O}_8$ . By replacing appropriate amounts of  $\text{SnCl}_4 \cdot 5\text{H}_2\text{O}$  by  $\text{ZrOCl}_2 \cdot 8\text{H}_2\text{O}$  we have been able to prepare cubic materials  $\text{Zr}_{1-x}\text{Sn}_x\text{Mo}_2\text{O}_8$  over the range  $0.2 \leq x \leq 1$  by this route. This A-site solubility range is significantly higher than has been possible in other  $\text{AM}_2\text{O}_8$  systems. Sample structure and composition have been determined by powder diffraction and Energy Dispersive X-ray spectroscopy (EDX) on selected samples. Materials with  $x < 1$  are typically slightly Sn deficient, which can be compensated by use of a small excess of Sn during synthesis. Accurate cell parameters for the cubic phases have been determined using a Si internal standard and are included in Figure 2b and in supporting information. For Zr-rich samples ( $x < \sim 0.4$ ) preparation of the cubic phase becomes progressively more difficult due to increased competition with the formation of trigonal phases. This is unsurprising given the literature on  $\text{ZrMo}_2\text{O}_8$  and the importance of proceeding via the so-called LT intermediate phase in accessing cubic  $\gamma$ - $\text{ZrMo}_2\text{O}_8$ <sup>42-44</sup>

Optimum kinetically-controlled synthetic conditions for accessing these metastable  $\text{AM}_2\text{O}_8$  materials have therefore been determined by in-situ X-ray diffraction studies. Figure 3a shows a typical experiment in which a series of diffraction patterns were recorded on warming a sample of amorphous  $\text{Zr}_{0.4}\text{Sn}_{0.6}\text{Mo}_2\text{O}_y(\text{OH})_{16-2-y} \cdot n\text{H}_2\text{O}$  from room temperature to 1120 K. 25% by mass of crystalline  $\text{Al}_2\text{O}_3$  was mixed with the sample as an inert internal standard to allow quantification of the amorphous content on heating. Figure 3b shows the quantitative phase analysis. From room temperature to  $\sim 670$  K the sample remains amorphous. Between  $\sim 670$  and 720 K cubic  $\text{Zr}_{0.4}\text{Sn}_{0.6}\text{Mo}_2\text{O}_8$  forms as the only crystalline phase. The amorphous content falls to close to zero within the precision of the experiment, indicating that crystalline  $\text{Zr}_{0.4}\text{Sn}_{0.6}\text{Mo}_2\text{O}_8$  is the principal phase present. No intermediate crystalline phases, such as the LT phase observed in the  $\text{ZrMo}_2\text{O}_8$  system, are seen. Above  $\sim 1000$  K cubic  $\text{Zr}_{0.4}\text{Sn}_{0.6}\text{Mo}_2\text{O}_8$  decomposes,  $\text{SnO}_2$  and  $\text{ZrO}_2$  related phases are formed and  $\text{MoO}_3$  is lost by volatilization.  $\text{MoO}_3$  loss is consistent with ex-situ studies of the synthesis of tin molybdenum oxides and explains the apparent rise in amorphous content at high temperatures.<sup>38</sup> Similar behavior is observed for samples with  $0.5 \leq x \leq 1$ . For  $0.2 \leq x \leq 0.5$  the cubic material can be formed as the major crystalline phase (up to  $\sim 85:15\%$  cubic: trigonal at  $x = 0.2$ ), though some amorphous component (10–20%) may still be present. Cell parameters of the cubic phase (see Supporting Information Figure S3) suggest a full range of solid solution is possible for  $0.2 \leq x \leq 1.0$ . Work is underway to try and improve phase purity at the Zr-rich end of the solid solution to allow

access to bulk cubic samples over the whole composition range.

Figure 2c shows thermal expansion data of a series of samples for  $0 \leq x \leq 1$  in the form of  $\Delta a/a_{300\text{ K}}$ . The thermal expansion of this system can be systematically controlled over the range  $\alpha_1 = -5.9(2)$  to  $+7.9(2) \times 10^{-6} \text{ K}^{-1}$  (12–500 K). Systems with approximately equal Sn:Zr ratios, have extremely low coefficients of expansion over the entire temperature range studied, with  $\text{Zr}_{0.4}\text{Sn}_{0.6}\text{Mo}_2\text{O}_8$  having essentially zero thermal expansion from 12 to 600 K ( $\alpha_{12-600} = -6(20) \times 10^{-8} \text{ K}^{-1}$ ).

This level of control of thermal expansion and contraction within a single cubic phase over such a wide temperature range is unprecedented. Previous studies on expansion control in materials such as  $\text{ZrV}_{2-x}\text{P}_x\text{O}_7$  have involved systems where end members both show positive thermal expansion close to room temperature and low/negative expansion is only achieved at significantly higher temperatures.<sup>45</sup>

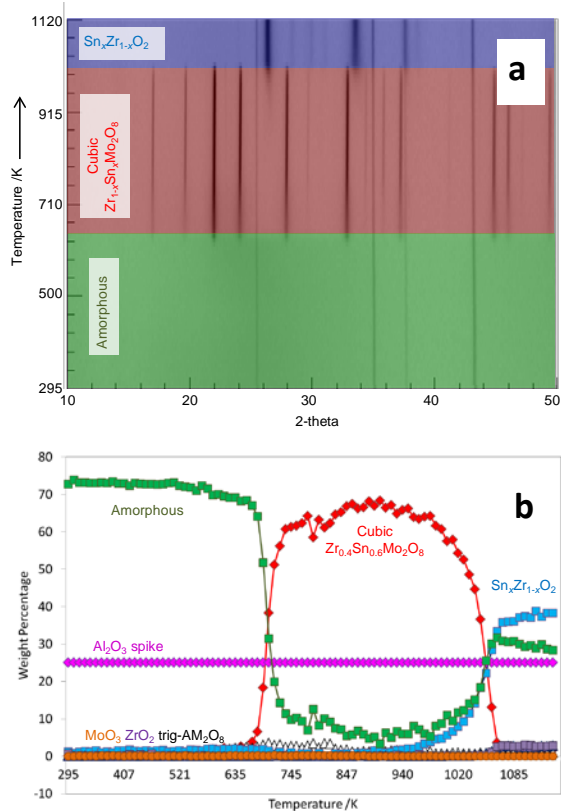


**Figure 3.** In situ diffraction study of  $\text{Zr}_{0.4}\text{Sn}_{0.6}\text{Mo}_2\text{O}_8$  synthesis. **a**, surface plot of powder diffraction on warming amorphous  $\text{Zr}_{0.4}\text{Sn}_{0.6}\text{Mo}_2\text{O}_8(\text{OH})_{16-2y}n\text{H}_2\text{O}$  mixed with 25% by weight  $\text{Al}_2\text{O}_3$  internal standard from room temperature to 1120 K. **b**, phase quantification by Rietveld refinement.

**Temperature- and Time-Dependent Structural Phase Transitions in Cubic  $\text{SnMo}_2\text{O}_8$ .** In addition to its role in allowing us to produce near-ZTE in cubic  $\text{AM}_2\text{O}_8$  materials, the  $x = 1$   $\alpha$ - $\text{SnMo}_2\text{O}_8$  material shows unexpected changes as a function of time and temperature which reveal new aspects of the structural chemistry of this important family. Firstly, thermal expansion studies on  $\alpha$ - $\text{SnMo}_2\text{O}_8$  reveal a volume-increasing phase transition between  $\sim 330$  and  $390$  K; we call the high temperature phase the  $\beta$  form. This behavior is again in contrast to other  $\text{AM}_2\text{O}_8$  systems where heating over

similar temperatures can lead to volume-decreasing phase transitions which are associated with a dynamic order-disorder phase transition of the orientation of pairs of  $2 \times \text{MO}_4$  tetrahedra along the cubic  $\langle 111 \rangle$  direction (see Figure 1a). In  $\text{ZrW}_2\text{O}_8$  this changes the symmetry from non-centrosymmetric  $P2_13$  in the ordered  $\alpha$ -form to centrosymmetric  $Pa\bar{3}$  in the disordered  $\beta$ -form.<sup>46</sup> Similar though less pronounced transitions are seen for  $\text{Zr}_{1-x}\text{Sn}_x\text{Mo}_2\text{O}_8$  with  $x < 1$ .

Repeated thermal expansion measurements on warming and cooling  $\text{SnMo}_2\text{O}_8$  through the  $\alpha$  to  $\beta$  phase transition showed that freshly prepared samples all had thermal expansion similar in form to Figure 2a, but that unusually large differences were observed between room temperature cell parameters depending on the sample's thermal history (see Supporting Information Figure S4). Cell parameters of samples held for extended periods at room temperature also often showed a small but measurable decrease in cell parameter over time (see Supporting Information Figure S7). This contraction occurred for samples sealed in glass capillaries and also for samples held under a dynamic vacuum of  $10^{-4}$  atm suggesting that it was not caused by water uptake as has been observed in other members of the  $\text{AM}_2\text{O}_8$  family.<sup>47,48</sup> This observation suggested that  $\alpha$ - $\text{SnMo}_2\text{O}_8$  could exist in a kinetically trapped glassy state related to the high temperature dynamically disordered form.

Figure 4 shows the results of a series of time- and temperature-dependent diffraction experiments designed to probe this behavior. A sample of  $\alpha$ - $\text{SnMo}_2\text{O}_8$  was heated from 300 to 500 K, quench-cooled in liquid nitrogen ( $< 30$  s to cool from 500 to 100 K) then held for 12 hour periods at 7 temperatures between 250 and 370 K; powder data were recorded in multiple 30 minute time slices at each temperature. Figure 4a shows all the cell parameters determined, plotted as a function of temperature. The time-zero 250 K cell parameter (8.9698 Å) suggests that quench-cooling is able to freeze in the high temperature form. Figure 4b (which shows the same data as a function of time) shows that there is then a small but significant reduction in cell parameter as the sample is held at constant temperature. On stepping the temperature to 270 K there is an initial increase in cell parameter (normal positive thermal expansion) followed by a further decrease during the isothermal treatment. The rate of contraction of  $\text{SnMo}_2\text{O}_8$  with time increases significantly with increasing temperature as expected for an activated process. A simple Arrhenius treatment assuming evolution to a constant state yields an apparent activation energy of  $33(2) \text{ kJ mol}^{-1}$  using data from 270–350 K. This compares with an  $E_A$  for oxygen migration via polyhedral rearrangement in  $\text{ZrW}_2\text{O}_8$  from solid state  $^{17}\text{O}$  NMR of  $24.5(5) \text{ kJ mol}^{-1}$  in  $\alpha$ - $\text{ZrW}_2\text{O}_8$ ,  $42(9)$  in  $\beta$ - $\text{ZrW}_2\text{O}_8$ <sup>21,49</sup> and  $34(5) \text{ kJ mol}^{-1}$  in  $\text{ZrWMoO}_8$ <sup>21</sup>

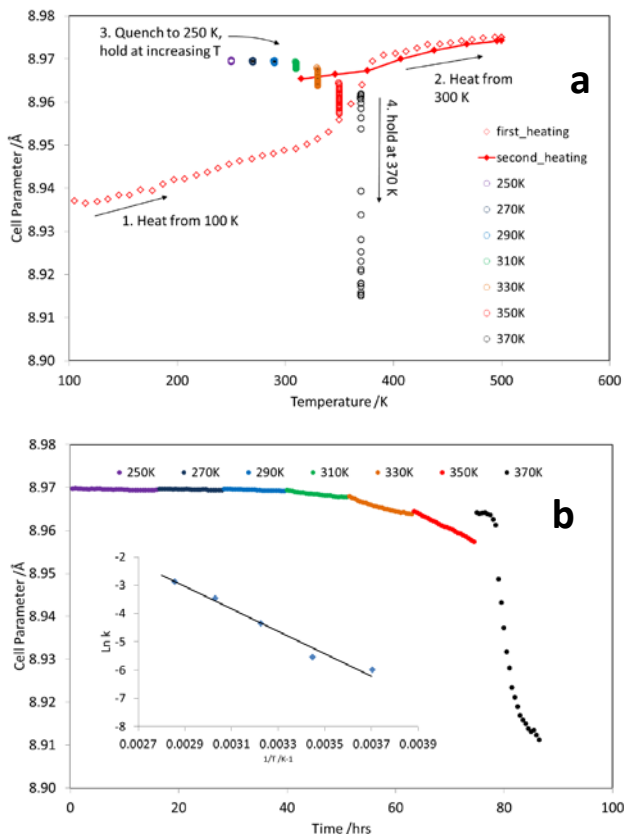


**Figure 4.** Oxygen ordering in  $\text{SnMo}_2\text{O}_8$ . **a**, cell parameter evolution on (1) heating  $\alpha$ - $\text{SnMo}_2\text{O}_8$  from 100 K to 500 K at 20 K/hr, (2) cooling to room temperature then heating to 500 K at 60 K/hr, (3) quenching from 500 K to 250 K then holding isothermally at increasing temperatures for 12 hour periods up to (4) 370 K. **b**, shows cell parameters from stage (3) of Figure 4a plotted as a function of experimental time; inset to **b** shows Arrhenius plot. Data were collected on a sample mounted in a 0.3 mm capillary on a Bruker d8 diffractometer operating in transmission mode with  $\text{Cu K}\alpha_{1/2}$  radiation.

The data in stage 3 of Figure 4a suggested that the cell parameters of a time- and temperature-evolved quench-cooled sample and a normal warmed sample would converge at  $\sim 370$  K & an equilibrium state would be reached. Initial isothermal data recorded at 370 K suggested this behavior with a  $\approx 8.962$  Å (start of stage 4 of Figure 4a). However, a large and rapid reduction in cell parameters ( $\Delta V \approx -1.7\%$ ) accompanied by marked broadening of several peaks in the diffraction pattern was observed after  $\sim 6$  hr at 370 K. On holding the sample at 400 K for 5 h the broadening evolved into a clear splitting of most reflections in the powder pattern. The peak splitting pattern observed is indicative of a complete phase transition to rhombohedral symmetry with a cell of  $a \approx 12.50$ ,  $c \approx 31.10$  Å with  $c/2a = 1.244$ , a 1.6% distortion from metrically cubic symmetry (transformation:  $[-110; 0-11; 222]$ ).<sup>50</sup> This rhombohedral phase remained stable on cooling to room temperature. Similar phase evolution was observed in a fresh sample of  $\alpha$ - $\text{SnMo}_2\text{O}_8$  warmed from room temperature. Figure 5a shows a surface plot of powder diffraction data collected for  $12 \times 30$  minutes at each of 10 temperatures from 360 to 450 K. Clear peak splitting indicative of the phase transition to rhombohedral symmetry is observed at  $\sim 390$  K followed by a sharp, first-order transi-

tion on further heating at  $\sim 440$  K back to the high temperature  $\beta$  form.

**Structural Relationships.** The fascinating thermal expansion properties of this system are intimately linked to its complex structural chemistry. Full crystallographic details of the structures and structural relationships between the different forms of  $\text{SnMo}_2\text{O}_8$  encountered will be published elsewhere, and we'll restrict discussion here to the gross changes that occur. We will denote the initial low temperature metrically cubic form as  $\alpha$ - $\text{SnMo}_2\text{O}_8$ , the rhombohedral form prepared by annealing at 400 K as  $\gamma$ - $\text{SnMo}_2\text{O}_8$  and the high temperature form as  $\beta$ - $\text{SnMo}_2\text{O}_8$ .

Powder neutron and single crystal X-ray diffraction data show that high temperature  $\beta$ - $\text{SnMo}_2\text{O}_8$  is cubic and isostructural with the  $Pa\bar{3}$  high temperature form of  $\beta$ - $\text{ZrW}_2\text{O}_8$  or room temperature  $\gamma$ - $\text{ZrMo}_2\text{O}_8$  (see Supporting Information). In this form the orientations of pairs of  $2 \times \text{MoO}_4$  tetrahedra are dynamically disordered along the cubic  $\langle 111 \rangle$  axes as shown in Figure 1a. Figure 6 shows that peak intensities in the X-ray powder diffraction patterns of low temperature  $\alpha$ - $\text{SnMo}_2\text{O}_8$  are very similar to those in the high temperature  $\beta$ -form indicating a strong similarity in the structures and suggesting that it has a predominantly disordered arrangement of  $\text{MoO}_4$  tetrahedra. Single crystal diffraction data reveal, however, extra reflections over those observed for the simple  $\beta$  structure at high temperature. All observed reflections could be indexed using a rhombohedral unit cell with  $a = 12.6$  and  $c = 31.0$  Å at 120K, which represents a doubling in the volume relative to the cubic cell, which would have  $a = 12.6$   $c = 15.5$  in this rhombohedral setting. By Rietveld or Pawley-fitting high resolution laboratory powder diffraction, no metric distortion of the  $\alpha$ - $\text{SnMo}_2\text{O}_8$  cell from cubic symmetry can be observed over its entire stability range ( $c/2a = 1.2252(3)$  compared to 1.2247 for undistorted cubic symmetry, Supporting Information Figure S6).

The transition from  $\alpha$  to  $\gamma$   $\text{SnMo}_2\text{O}_8$  at  $\sim 400$  K leads to marked distortion in the cell metric ( $a = 12.503$   $c = 31.0958$ ,  $c/2a = 1.244$ , a 1.6 % distortion) giving clear peak splitting in the powder pattern and small but observable changes in the integrated intensity of sets of related pseudo-cubic reflections (e.g. around a 10% increase for stronger reflections, a doubling in intensity for the weaker 302 family, see Figure 6). The intensity changes indicate a more marked structural change and powder data of  $\gamma$ - $\text{SnMo}_2\text{O}_8$  can be fitted well by Rietveld refinement of a model with  $R\bar{3}$  symmetry in which the  $2 \times \text{MoO}_4$  tetrahedra along the threefold axes of the original cubic unit cell adopt an ordered arrangement. Rietveld plots are included in Figure 5b and Supporting Information. The ordering arrangement differs from that observed in  $\alpha$ - $\text{ZrW}_2\text{O}_8$  and, using a symmetry-adopted distortion mode description,<sup>51</sup> can be described with an  $R1+R3+$  irrep as opposed to the  $\Gamma 1-$  irrep that describes ordering in  $\text{ZrW}_2\text{O}_8$ . The different ordering pattern is highlighted in Figure 1. In Figure 1b the tetrahedral sites occupied in  $\gamma$ - $\text{SnMo}_2\text{O}_8$  have been shaded as to whether they have the same orientation as in  $\alpha$ - $\text{ZrW}_2\text{O}_8$  (yellow) or reversed (pink).  $\gamma$ - $\text{SnMo}_2\text{O}_8$  itself shows positive thermal expansion from 312 to 412 K with  $\alpha_1 = 1.87 \times 10^{-5} \text{ K}^{-1}$  and a  $c/2a$  ratio which falls smoothly to 1.241 on heating (Supporting Information Figure S6) before transforming to the  $\beta$  form at  $\sim 440$  K.

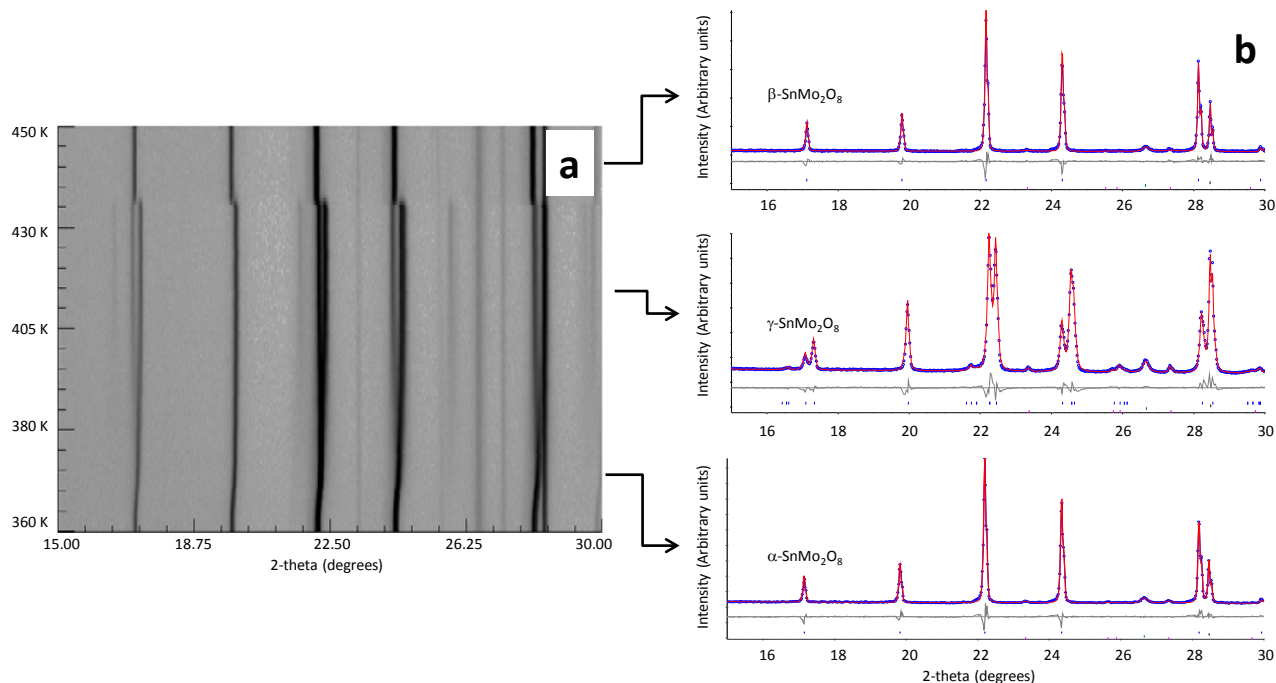


**Figure 5.** **a** shows a surface plot of powder diffraction data of  $\text{SnMo}_2\text{O}_8$  held for 6 hours as temperature increased in 10 K intervals from 360–450 K. **b** shows Rietveld refinements of the  $\alpha$ -, cubic- $\beta$  and rhombohedral- $\gamma$  structures.  $\gamma$  refinement performed using data collected on a sample cooled back to room temperature. A Si internal standard (lower tick marks) was used. Observed data in blue, calculated in red, difference in grey. Small vertical bars show positions of allowed hkl reflections. Data were collected with Cu  $K\alpha_{1/2}$  radiation reflection mode.

The observation of this phase transition to a  $2 \times \text{MoO}_4$  ordered structure with a significantly smaller volume than the  $\alpha$  or  $\gamma$  forms helps explain the unusual time dependent behavior observed in cell volumes of Figure 4. The energy landscape of pseudo-cubic  $\text{SnMo}_2\text{O}_8$  is such that an entropically stabilized dynamically disordered form is stable above  $\sim 400$  K. At lower temperature the fully ordered  $\gamma$  form is presumably the thermodynamically stable phase (or at least the locally most stable phase without the extensive reconstruction required for phase segregation or formation of a different polymorph). The rate of  $\text{MoO}_4$  reorientation in the structure is sufficiently slow that it is easy to freeze in the high temperature disorder in the  $\alpha$  form, with extremely long time periods required to access the stable  $\gamma$  structure at low temperatures. Partial  $\text{MoO}_4$  ordering presumably occurs in  $\alpha$ - $\text{SnMo}_2\text{O}_8$  such that the local structure resembles the lower-volume  $\gamma$ - $\text{SnMo}_2\text{O}_8$  structure. The unwinding of local cooperative polyhedral tilts would contribute to the PTE of  $\alpha$ - $\text{SnMo}_2\text{O}_8$  at low temperature and the gradual disruption of local order will cause the volume expansion at the  $\alpha$  to  $\beta$  transition. We have treated ZTE  $\text{Zr}_{1-x}\text{Sn}_x\text{Mo}_2\text{O}_8$  with  $x \sim 0.5$  to similar heating regimes as shown in Figure 5a but have not observed transitions to the  $\gamma$  structure.

## CONCLUSION

$\text{Zr}_{1-x}\text{Sn}_x\text{Mo}_2\text{O}_8$  is a fascinating system that shows a number of surprises. Firstly the  $x = 1$  phase is unique amongst  $\text{AM}_2\text{O}_8$  materials in showing PTE in all its forms ( $\alpha$ ,  $\beta$  and  $\gamma$ ). We presume the origins of the PTE arises from a number of contributions. Firstly the 2.6% smaller cell volume rela-

tive to  $\text{ZrW}_2\text{O}_8$  and increased stiffness of smaller  $\text{SnO}_6$  octahedra are sufficient that negative-Grüneisen-parameter phonon modes are overwhelmed by positive modes. A general correlation between NTE and cation size has been observed in other systems such as  $\text{A}_2(\text{MO}_4)_3$  and  $\text{AP}_2\text{O}_7$  materials.<sup>5</sup> There will also be contributions from the unwinding of any cooperative polyhedral tilts allowed in the lower symmetry  $\alpha$  phase and due to the evolution of short range order of  $\text{MoO}_4$  groups. The intrinsic volume and thermal expansion properties of  $\text{SnMo}_2\text{O}_8$  are strongly influenced by the precise pattern of ordering of  $\text{MoO}_4$  tetrahedra within the structure, with a range of ordered and disordered configurations accessible close to room temperature. Structural reorientation of the  $\text{MoO}_4$  groups occurs from 250 K but becomes sufficiently accessible at 400 K for formation of the ordered  $\gamma$  structure, which has a configuration unique amongst these materials.

The identification of a PTE phase isostructural to the NTE  $\text{AM}_2\text{O}_8$  materials has led us to develop a low temperature route allowing a far greater range of solid solution on the A site of a cubic  $\text{AM}_2\text{O}_8$  system than has been achieved before. We can thereby systematically control isotropic expansion properties of  $\text{Zr}_{1-x}\text{Sn}_x\text{Mo}_2\text{O}_8$  from positive to negative values, including zero.

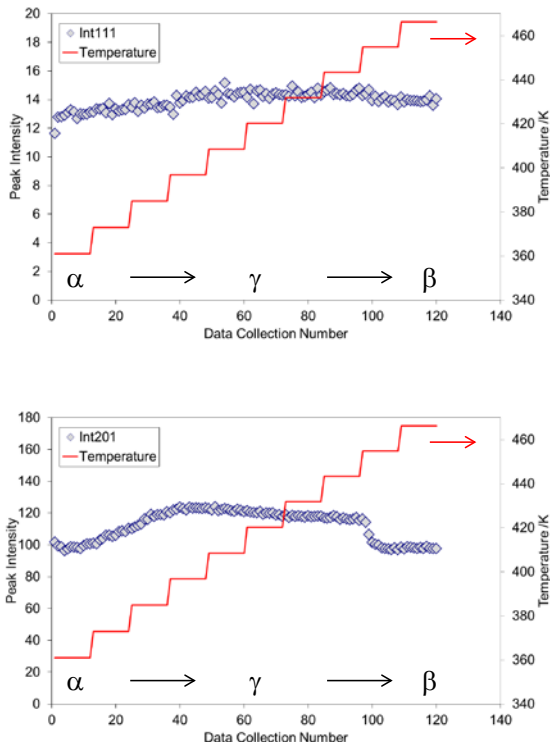


**Figure 6.** Intensities of representative X-ray peaks as  $\alpha$ - $\text{SnMo}_2\text{O}_8$  is gradually heated from 360 to 460 K, as shown in Figure 5a. Plots show the summed intensities of families of peaks related to individual hkl reflections in the cubic  $\beta$ -phase. 111 reflection shows minimal changes with temperature. 201 (and other peaks – see SI) show significant intensity changes on entering the rhombohedral  $\gamma$ -phase associated with ordering of  $2 \times \text{MoO}_4$  tetrahedra. Peak intensities revert to values similar to those in the  $\alpha$ -phase on passing through the  $\gamma$  to  $\beta$  transition. Temperature profile is shown on the right hand scale.

## ASSOCIATED CONTENT

### SUPPORTING INFORMATION

Supporting information contains full details on the Rietveld refinement of neutron diffraction data for  $\beta$ - $\text{SnMo}_2\text{O}_8$ ; data similar to Figure 6 for more reflections during the  $\alpha$  to  $\beta$  to  $\gamma$  transition; Vegard's law plots of cell dependence on  $x$  for  $\text{Zr}_{1-x}\text{Sn}_x\text{Mo}_2\text{O}_8$  samples; the temperature dependence of cell parameters for  $\text{SnMo}_2\text{O}_8$  samples with a variety of thermal histories; details of Rietveld refinement for  $\gamma$ - $\text{SnMo}_2\text{O}_8$ ; and information on the variation in cell parameters and  $c/2a$  ratio as samples are cycled through the  $\alpha$  to  $\gamma$  to  $\beta$  to  $\alpha$  phase transitions. This material is available free of charge via the Internet at <http://pubs.acs.org>.

### AUTHOR INFORMATION

#### Corresponding Author

john.evans@durham.ac.uk

### ACKNOWLEDGMENT

We thank STFC for access to the ISIS facility for neutron scattering experiments and the Diamond Light Source for single

crystal experiments. We thank the EPSRC and Durham University for provision of equipment underpinning the work reported.

## REFERENCES

- (1) Sleight, A. W. *Inorganic Chemistry* **1998**, *37*, 2854.
- (2) Barrera, G. D.; Bruno, J. A. O.; Barron, T. H. K.; Allan, N. L. *Journal of Physics-Condensed Matter* **2005**, *17*, R217.
- (3) Evans, J. S. O. *Journal of the Chemical Society-Dalton Transactions* **1999**, 3317.
- (4) Takenaka, K. *Science and Technology of Advanced Materials* **2012**, *13*.
- (5) Lind, C. *Materials* **2012**, *5*, 1125.
- (6) Arvanitidis, J.; Papagelis, K.; Margadonna, S.; Prassides, K.; Fitch, A. N. *Nature* **2003**, *425*, 599.
- (7) Azuma, M.; Chen, W.-t.; Seki, H.; Czapski, M.; Olga, S.; Oka, K.; Mizumaki, M.; Watanuki, T.; Ishimatsu, N.; Kawamura, N.; Ishiwata, S.; Tucker, M. G.; Shimakawa, Y.; Attfield, J. P. *Nature Communications* **2011**, *2*.
- (8) Margadonna, S.; Prassides, K.; Fitch, A. N.; Salvador, J. R.; Kanatzidis, M. G. *Journal of the American Chemical Society* **2004**, *126*, 4498.
- (9) Salvador, J. R.; Gu, F.; Hogan, T.; Kanatzidis, M. G. *Nature* **2003**, *425*, 702.
- (10) Guillaume, C. E. C. *R. Acad. Sci* **1897**, *125*, 235.
- (11) Takenaka, K.; Takagi, H. *Applied Physics Letters* **2005**, *87*.
- (12) Zheng, X. G.; Kubozono, H.; Yamada, H.; Kato, K.; Ishiwata, Y.; Xu, C. N. *Nature Nanotechnology* **2008**, *3*, 724.
- (13) Takenaka, K.; Takagi, H. *Applied Physics Letters* **2009**, *94*.
- (14) Miller, W.; Smith, C. W.; Mackenzie, D. S.; Evans, K. E. *Journal of Materials Science* **2009**, *44*, 5441.
- (15) Sawhill, S.; Savrun, E. *Ceramics International* **2012**, *38*, 1981.
- (16) Tao, J. Z.; Sleight, A. W. *Journal of Solid State Chemistry* **2003**, *173*, 45.
- (17) Morelock, C. R.; Greve, B. K.; Cetinkol, M.; Chapman, K. W.; Chupas, P. J.; Wilkinson, A. P. *Chem. Mat.* **2013**, *25*, 1900.
- (18) Mary, T. A.; Evans, J. S. O.; Vogt, T.; Sleight, A. W. *Science* **1996**, *272*, 90.
- (19) Evans, J. S. O.; Mary, T. A.; Vogt, T.; Subramanian, M. A.; Sleight, A. W. *Chem. Mat.* **1996**, *8*, 2809.
- (20) Allen, S.; Evans, J. S. O. *Phys. Rev. B* **2003**, *68*, 134101.
- (21) Allen, S.; Evans, J. S. O. *Journal of Materials Chemistry* **2004**, *14*, 151.
- (22) The Gruneisen parameter is defined as  $d(\ln \nu)/dV$  where  $\nu$  is the vibrational frequency.
- (23) Heine, V.; Welche, P. R. L.; Dove, M. T. *Journal of the American Ceramic Society* **1999**, *82*, 1793.
- (24) Pryde, A. K. A.; Hammonds, K. D.; Dove, M. T.; Heine, V.; Gale, J. D.; Warren, M. C. *Journal of Physics-Condensed Matter* **1996**, *8*, 10973.
- (25) Tucker, M. G.; Keen, D. A.; Evans, J. S. O.; Dove, M. T. *Journal of Physics-Condensed Matter* **2007**, *19*.
- (26) Chang, L. L. Y.; Scroger, M. G.; Phillips, B. *Journal of the American Ceramic Society* **1967**, *50*, 211.
- (27) Readman, J. E.; Lister, S. E.; Peters, L.; Wright, J.; Evans, J. S. O. *Journal of the American Chemical Society* **2009**, *131*, 17560.
- (28) De Buysser, K.; Van Driessche, I.; Putte, B. V.; Schaubroeck, J.; Hoste, S. *Journal of Solid State Chemistry* **2007**, *180*, 2310.
- (29) De Meyer, C.; Bouree, F.; Evans, J. S. O.; De Buysser, K.; Bruneel, E.; Van Driessche, I.; Hoste, S. *Journal of Materials Chemistry* **2004**, *14*, 2988.
- (30) Guo, F.-L.; Ma, H.; Yang, X.-J.; Deng, X.-B.; Zhao, X.-H. *Chinese Journal of Inorganic Chemistry* **2011**, *27*, 2061.
- (31) Hashimoto, T.; Kuwahara, J.; Yoshida, T.; Nashimoto, M.; Takahashi, Y.; Takahashi, K.; Morito, Y. *Solid State Communications* **2004**, *131*, 217.

- (32) Li, H.-H.; Han, J.-S.; Ma, H.; Huang, L.; Zhao, X.-H. *Journal of Solid State Chemistry* **2007**, *180*, 852.
- (33) Nakajima, N.; Yamamura, Y.; Tsuji, T. *Journal of Thermal Analysis and Calorimetry* **2002**, *70*, 337.
- (34) Nakajima, N.; Yamamura, Y.; Tsuji, T. *Solid State Communications* **2003**, *128*, 193.
- (35) Yamamura, Y.; Nakajima, N.; Tsuji, T.; Kojima, A.; Kuroiwa, Y.; Sawada, A.; Aoyagi, S.; Kasatani, H. *Phys. Rev. B* **2004**, *70*.
- (36) Yamamura, Y.; Kato, M.; Tsuji, T. *Thermochimica Acta* **2005**, *431*, 24.
- (37) Safonov, V. V.; Porotnikov, N. V.; Chaban, N. G. *Zhurnal Neorganicheskoi Khimii* **1983**, *28*, 811.
- (38) Berry, F. J.; Hallett, C. *Inorganica Chimica Acta-Articles and Letters* **1985**, *98*, 135.
- (39) Feja, S., Technische Universitat Dresden, 2004.
- (40) Buiten, J. *Polyhedron* **1988**, *7*, 585.
- (41) Stinton, G. W.; Evans, J. S. O. *Journal of Applied Crystallography* **2007**, *40*, 87.
- (42) Lind, C.; Wilkinson, A. P.; Hu, Z. B.; Short, S.; Jorgensen, J. D. *Chem. Mat.* **1998**, *10*, 2335.
- (43) Lind, C.; Wilkinson, A. P.; Rawn, C. J.; Payzant, E. A. *Journal of Materials Chemistry* **2001**, *11*, 3354.
- (44) Allen, S.; Warmingham, N. R.; Gover, R. K. B.; Evans, J. S. O. *Chem. Mat.* **2003**, *15*, 3406.
- (45) Korhuis, V.; Khosrovani, N.; Sleight, A. W.; Roberts, N.; Dupree, R.; Warren, W. W. *Chem. Mat.* **1995**, *7*, 412.
- (46) Evans, J. S. O.; David, W. I. F.; Sleight, A. W. *Acta Crystallogr. Sect. B-Struct. Sci.* **1999**, *55*, 333.
- (47) Banek, N. A.; Baiz, H. I.; Latigo, A.; Lind, C. *Journal of the American Chemical Society* **2010**, *132*, 8278.
- (48) Duan, N.; Kameswari, U.; Sleight, A. W. *Journal of the American Chemical Society* **1999**, *121*, 10432.
- (49) Hampson, M. R.; Evans, J. S. O.; Hodgkinson, P. *Journal of the American Chemical Society* **2005**, *127*, 15175.
- (50) A metrically cubic rhombohedral cell in hexagonal setting has a c/a ratio of  $(3/2)^{0.5}$  giving a c/2a ratio of 1.225 for a cell metrically undistorted from cubic but with the cell volume observed here.
- (51) Campbell, B. J.; Stokes, H. T.; Tanner, D. E.; Hatch, D. M. *Journal of Applied Crystallography* **2006**, *39*, 607.

# Table of Contents artwork

